





Thermal cycling induced alteration of the stacking order and spin-flip in the room temperature van der Waals magnet $\text{Fe}_{5-\delta}\text{GeTe}_2$

Xiang Chen ^{1,2,*}, Wei Tian ³, Yu He,^{4,2,1} Hongrui Zhang ⁵, Tyler L. Werner,⁴ Saul Lapidus,⁶ Jacob P. C. Ruff,⁷ Ramamoorthy Ramesh ^{5,1,2} and Robert J. Birgeneau^{2,1,5}

¹Materials Science Division, Lawrence Berkeley National Lab, Berkeley, California 94720, USA

²Physics Department, University of California, Berkeley, California 94720, USA

³Neutron Scattering Division, Oak Ridge National Laboratory, Oak Ridge, Tennessee 37831, USA

⁴Department of Applied Physics, Yale University, New Haven, Connecticut, 06511, USA

⁵Department of Materials Science and Engineering, University of California, Berkeley, California 94720, USA

⁶Advanced Photon Source, Argonne National Laboratory, Argonne, Illinois 60439, USA

⁷Cornell High Energy Synchrotron Source, Cornell University, Ithaca, New York 14853, USA



(Received 9 September 2022; accepted 11 April 2023; published 24 April 2023)

The magnetic properties of the quasi-two-dimensional van der Waals magnet $\text{Fe}_{5-\delta}\text{GeTe}_2$ (F5GT), which has a high ferromagnetic ordering temperature $T_C \sim 315$ K, remain to be better understood. It has been demonstrated that the magnetization of F5GT is sensitive to both the Fe deficiency δ and the thermal-cycling history. Here, we investigate the structural and magnetic properties of F5GT single crystals with a minimal Fe deficiency ($|\delta| \leq 0.1$), utilizing combined x-ray and neutron scattering techniques. Our study reveals that the quenched F5GT single crystals experience an irreversible, first-order transition at $T_S \sim 110$ K upon first cooling, where the stacking order partly or entirely converts from ABC-stacking order to AA-stacking order. Importantly, the magnetic properties, including the magnetic moment direction and the enhanced T_C after the thermal cycling, are intimately related to the alteration of the stacking order. Our work highlights the significant influence of the lattice symmetry to the magnetism in F5GT.

DOI: [10.1103/PhysRevMaterials.7.044411](https://doi.org/10.1103/PhysRevMaterials.7.044411)

I. INTRODUCTION

The quasi-two-dimensional (quasi-2D) van der Waals (vdW) magnets are prominent systems for studying low-dimensional magnetism and anomalous transport behaviors [1–8]. Among them, the itinerant $\text{Fe}_{5-\delta}\text{GeTe}_2$ (F5GT) system is particularly interesting because of its advantageous characteristics for potential room temperature (RT) spintronic applications [9–13]. The bulk form of F5GT has a near RT ferromagnetic (FM) transition temperature $T_C \approx 275\text{--}330$ K [9–12, 14–19]. Owing to the coupling between the electronic and magnetic degrees of freedom, and the tunable sample thickness, the magnetic properties of F5GT are highly susceptible to perturbations [20–31]. For example, enhanced FM transition temperatures, from RT to 400 K and beyond, can be achieved by replacing Fe with either cobalt (Co) or nickel (Ni) [24–28], or through applying high pressure [30]. Also, a magnetic phase transition from a FM to an antiferromagnetic (AFM) ground state can be obtained via Co doping or by voltage induced charge doping [24, 26, 29]. Interestingly, topological spin textures have been realized via engineering the lattice symmetry by Co doping or tuning the sample thickness [26, 27, 31]. The aforementioned observations highlight the immense capacity for exploring both novel physical phenomena and technological applications in F5GT.

Despite the large amount of research directed at characterizing the magnetism in F5GT, its magnetic ground state remains contested [10–12, 14, 16, 30]. Specifically, conflicting suggestions about the spin structure have been reported, ranging from out-of-plane FM [10, 12] to in-plane FM [11] to ferrimagnetic order [16]. This is partly due to the experimental techniques utilized for investigating the magnetic properties in F5GT which are either only surface sensitive or indirect probes of the microscopic magnetic structure, such as magnetic force microscopy, nitrogen-vacancy center magnetometry, and magnetotransport measurements [11, 14, 19, 30]. Further complexity is added because the magnetism of F5GT is sensitive to both the iron (Fe) deficiency ($\delta \geq 0$), especially the half-occupied Fe1 site, and the growth conditions during the crystal synthesis [12]. Therefore, it is important to have a thorough investigation of the microscopic lattice and magnetic structure in F5GT. Here, we utilize combined x-ray and neutron scattering techniques to study the bulk properties of F5GT single crystals. Our work indicates that the quenched F5GT single crystals, which exhibit thermal-cycling history dependencies according to magnetization measurements, actually undergo a first-order structural transition at $T_S \sim 110$ K upon first cooling [12]. During this irreversible process (< 400 K), the stacking order of the sample partly or completely converts from ABC-stacking order to AA-stacking order. Our neutron diffraction data indicate that the spin moment direction is directly controlled by the stacking order of the lattice, likely resulting from the strong magnetoelastic

*xiangchen@berkeley.edu

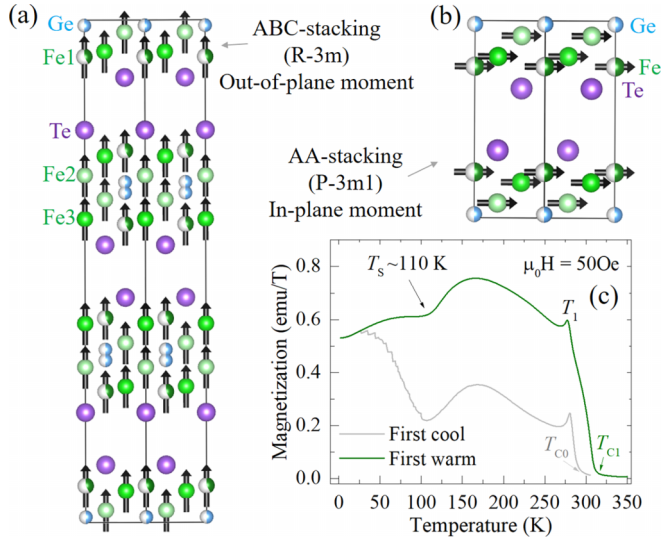


FIG. 1. (a) and (b) The crystal structure of Fe_5GeTe_2 (F5GT) with two different types of stacking order: (a) ABC-stacking order with the space group (SG) $R\bar{3}m$ and (b) AA-stacking order with the SG $P\bar{3}m1$ [24,26,27]. (c) Thermal-cycling history dependence of the in-plane magnetization of the quenched F5GT single crystals. Prior to the first cooling process, the ferromagnetic onset temperature T_{Co} is ~ 285 K (gray line), which is enhanced to $T_{C1} \sim 310$ K after cooling below $T_S \sim 110$ K (green line).

coupling and the interlayer exchange couplings. Our study highlights the significance of the stacking order and the interlayer couplings in determining the magnetic ground state of F5GT.

II. EXPERIMENTAL RESULTS

Single crystals of F5GT were obtained via the chemical vapor transfer technique and quenched at 750°C to improve the sample quality during the last step of the synthesis [10,12,26,27]. The cation deficiency ($|\delta| \leq 0.1$) of the crystals, verified by energy dispersive x-ray spectroscopy, indicates that our samples are nearly stoichiometric. The x-ray scattering experiments were carried out at 44 keV at beamline QM2 of the Cornell High Energy Synchrotron Source (CHESS). A Pilatus 6M area detector was used to collect the diffraction patterns with the sample rotated 365° around three different axes at 0.1° step and 0.1 s/frame data rates at each temperature. Elastic neutron scattering measurements were carried out using the 14.6-meV fixed-incident-energy triple-axis spectrometer HB-1A of the High Flux Isotope Reactor (HFIR) at Oak Ridge National Laboratory, with a collimation of $40'40'40'-80'$. For unpolarized neutrons, the nuclear and magnetic contributions to the structure factor are additive and the cross-term cancels, which is a significant advantage for magnetic neutron studies. For better comparison, the Bragg peaks $\mathbf{Q} = (H \frac{4\pi}{\sqrt{3}a}, K \frac{4\pi}{\sqrt{3}b}, L \frac{2\pi}{c})$ are defined in reciprocal lattice units (r.l.u.) with lattice parameters $a = b \approx 4.03$ Å and $c \approx 29.2$ Å for both ABC-stacking and AA-stacking ordered domains of F5GT [Figs. 1(a) and 1(b)]. The single crystals were quenched to RT and then used for the temperature-dependent magnetometry, x-ray scattering, and neutron scattering experiments.

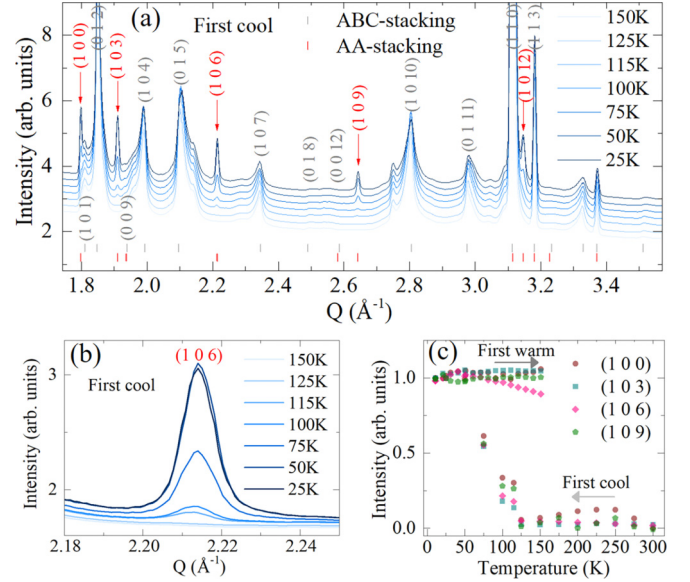


FIG. 2. (a) Temperature dependence of the x-ray diffraction pattern of F5GT, during the “first cool” procedure, collected with a decreasing temperature sequence. Vertical lines indicate the peak positions predicted by the two different models: ABC-stacking order with the SG $R\bar{3}m$ (gray) and AA-stacking with the SG $P\bar{3}m1$ (red). Emerging peaks below $T_S \sim 110$ K are marked and labeled in red. (b) Magnified view of the (1, 0, 6) peak at select temperatures. (c) Temperature dependence of the normalized peak intensity at select peaks $\mathbf{Q}_{AA} = (1, 0, 3N)$ ($N = 0, 1, 2, \text{ and } 3$).

Consistent with the reported results [12], the quenched F5GT single crystal exhibits a thermal history dependence as observed in the magnetization measurement [Fig. 1(c)]. Prior to any cooling process, the F5GT sample has a magnetic onset temperature of $T_{Co} \sim 285$ K [Fig. 1(c), gray line]. Upon the first cooling process from RT down to temperature $T = 2$ K (labeled as “first cool”), the F5GT sample experiences an irreversible, first-order structural transition at $T_S \sim 110$ K, as indicated by the large dip in the magnetization data [Fig. 1(c)]. After this initial cooling process, the F5GT sample is warmed up (labeled as “first warm” or “thermally cycled”) and has a permanently (without warming up to 400 K) enhanced magnetic transition temperature of $T_{C1} \sim 310$ K [Fig. 1(c), green line]. Further thermal cycling (either cooling or warming) of the crystal, as long as it is below ~ 550 K, does not affect the magnetization [12].

To understand the microscopic origin of the thermal history dependence of the magnetization, we first examine the structural properties of the quenched F5GT samples through single-crystal x-ray diffraction (XRD), which presents minimum external perturbation to the sample. Single crystals are favored for characterizing the lattice structure of the vdW materials, because undesired stacking faults are frequently produced during the sample preparation for the commonly used powder XRD. A freshly quenched F5GT single crystal was subjected to an identical thermal treatment: the measurement was performed at RT first, gradually cooled down to $T = 10$ K (first cool), and then slowly warmed up (first warm) towards RT. Figure 2(a) shows the x-ray scattering intensity plotted as a function of momentum Q during the first cool pro-

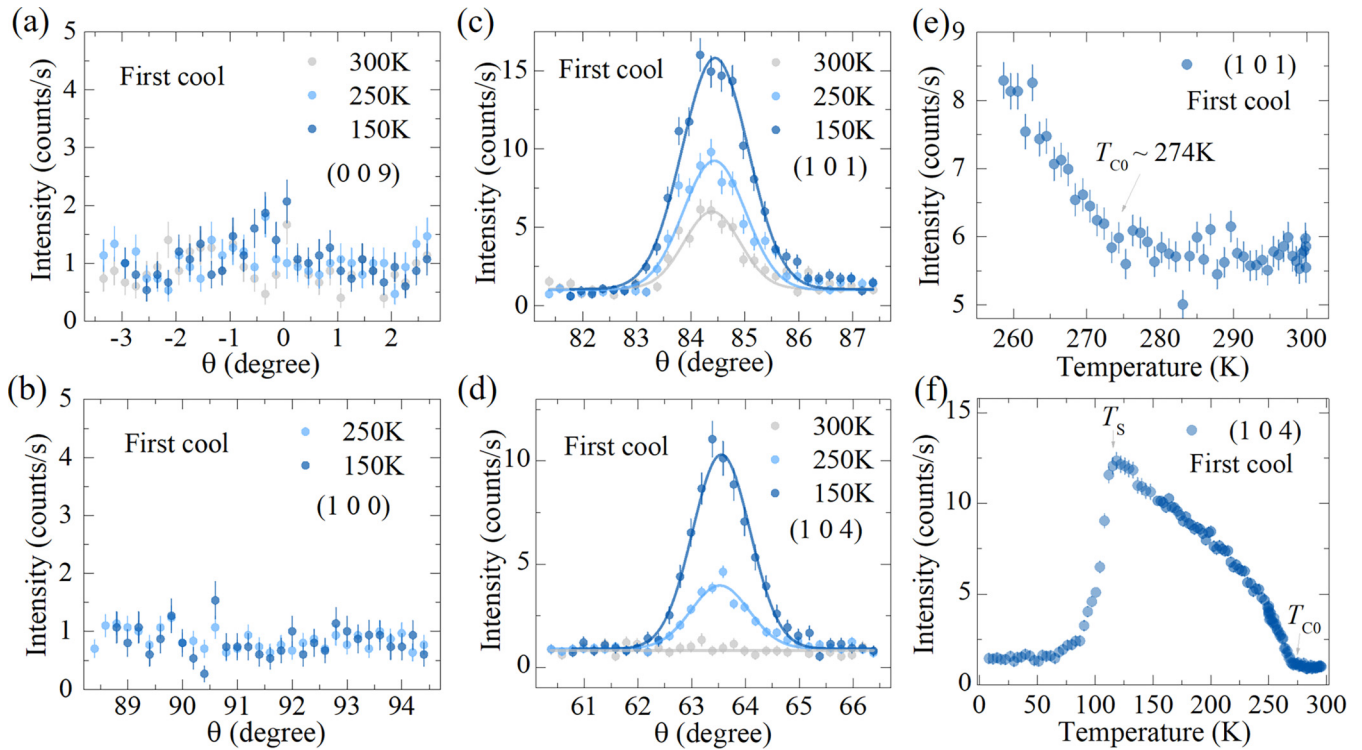


FIG. 3. Temperature dependence of the neutron diffraction peaks of F5GT during the first cool process. (a)–(d) Rocking scans at select Bragg peak positions: (a) (0, 0, 9); (b) (1, 0, 0); (c) (1, 0, 1); and (d) (1, 0, 4). Solid lines in panels (c) and (d) are Gaussian fits to the data. (e) and (f) Temperature dependence of the (1, 0, 1) peak (e) and the (1, 0, 4) peak (f), with the same magnetic transition temperature of $T_{c0} \sim 274$ K. The structural transition at T_S is reflected by the sharp decrease of the (1, 0, 4) peak intensity in panel (f). In panels (a)–(d), θ is the motor angle, which is proportional to the θ angle of the rocking scans.

cess. The observed peaks at RT can be well indexed with the space group (SG) $R\bar{3}m$ [Fig. 1(a)] [10], indicated by the gray vertical lines and the labeled peaks. This is consistent with the rhombohedral layer stacking, labeled as ABC-stacking [Fig. 1(a)] [10]. Interestingly, a new set of peaks emerges below $T_S \sim 110$ K during the first cool process (Fig. 2). While the peaks associated with the ABC-stacking order are only weakly suppressed in magnitude with decreasing temperature, the intensities of the new peaks become stronger and stabilize at the lowest temperature, as indicated by the temperature-dependent, normalized intensity of the selected peaks in Fig. 2(c). After the first cool process, the diffraction pattern only displays a weak temperature dependence with respect to further thermal cycling, agreeing with the permanent change evident from the magnetization measurements [12]. Some minor peaks are present on the shoulders of the main Bragg peaks, but barely display any temperature dependence during the whole temperature treatment. These minor peaks might be due to impurity phase(s) and/or stacking disorders during the sample synthesis; they are also shown to be present in the reported XRD studies [9,12].

The new peaks evidenced from the x-ray scattering measurement, indicated and labeled in red in Fig. 2(a), can be well indexed with the SG $P\bar{3}m1$, signaling the formation of a closely related type of stacking order, i.e., AA-stacking [Fig. 1(b)], as similarly observed in either Co- or Ni-doped F5GT samples [24,26,28]. The two types of stacking orders in F5GT, i.e., ABC-stacking and AA-stacking, share the same motif while they only differ marginally through

the stacking configuration along the lattice c direction. In the AA-stacking order with primitive centering [Fig. 1(b)], the lattice c of the unit cell should be $1/3$ of the lattice c with the ABC-stacking order. However, to maintain directly comparable Miller indices, a similar lattice $c \approx 29.2$ Å is used for both AA-stacking and ABC-stacking orders here. The direct benefit is the clear distinction between the two types of stacking orders in reciprocal space for the scattering measurement (Figs. 2–5). For the ABC-stacking order, the (1, 0, L) type of nuclear Bragg peaks can only be observed when $L \neq 3N$ ($L = \text{integers}$ and $N = 0, 1, 2, \dots$). Meanwhile, for the AA-stacking order indexed with this tripled lattice c , any allowed nuclear Bragg peak (H, K, L) must satisfy $L = 3N$ ($N = 0, 1, 2, \dots$). Therefore, for the (1, 0, L) type of nuclear Bragg peaks, the $\mathbf{Q}_{AA} = (1, 0, 3N)$ ($N = 0, 1, 2, \dots$) positions will only be allowed in the AA-stacking ordered domains, while the $\mathbf{Q}_{ABC} = (1, 0, 3N \pm 1)$ ($N = 0, 1, 2, \dots$) reflections will only be possible in the ABC-stacking ordered domains [Fig. 5(a)]. A sharp distinction between the two types of stacking orders can be readily recognized by inspecting the (1, 0, L) type of structural peaks [Fig. 5(a)]. Clearly, as shown in Fig. 2, the quenched F5GT crystal only has the ABC-stacking order prior to the first cool process because of the absence of the \mathbf{Q}_{AA} type of Bragg peaks. After the initial cooling below T_S , the emergence of the \mathbf{Q}_{AA} type of Bragg peaks, such as the (1, 0, 6) peak shown in Fig. 2(b), indicates the partial conversion from ABC-stacking order to AA-stacking order, which permanently remains so thereafter.

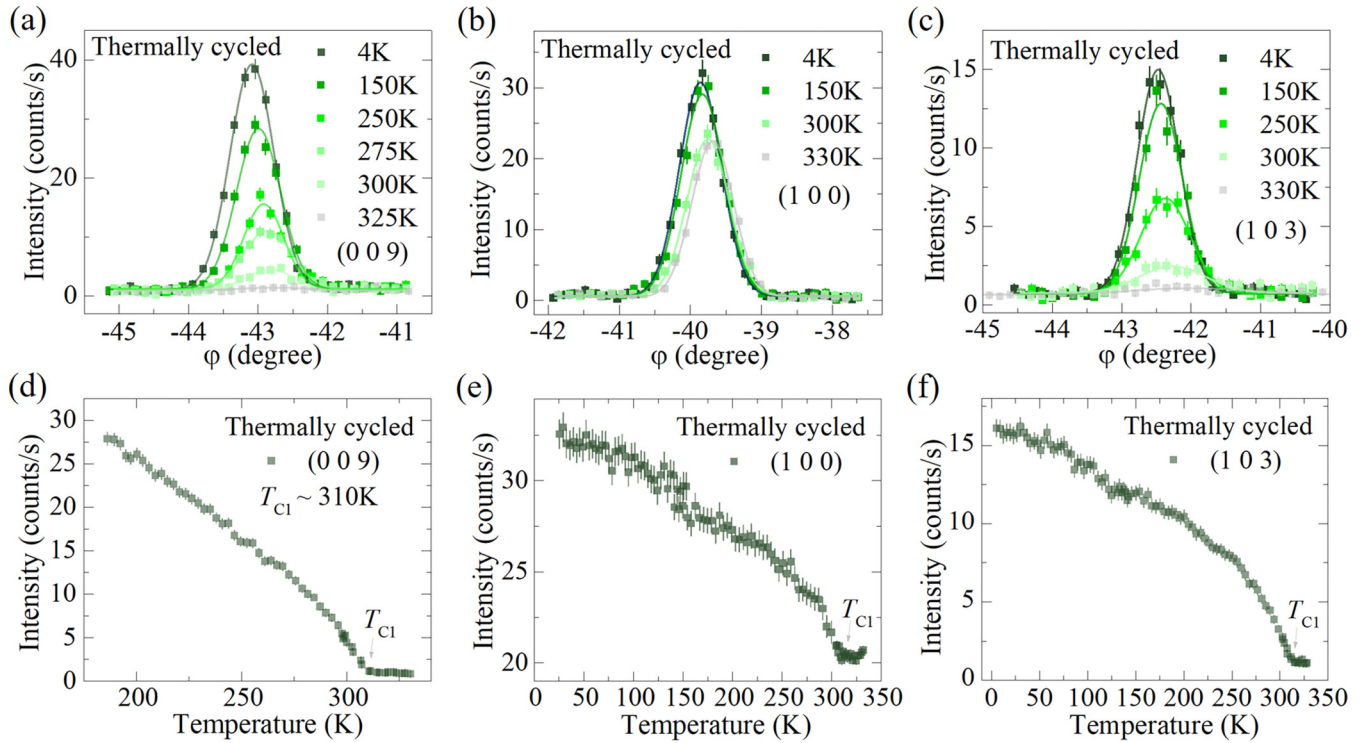


FIG. 4. Temperature dependence of the neutron diffraction peaks of F5GT after the sample is thermally cycled. (a)–(c) Radial scans at select Bragg peak positions: (a) (0, 0, 9), (b) (1, 0, 0), and (c) (1, 0, 3). Solid lines are Gaussian fits to the data. (d)–(f) Temperature dependence of the select Bragg peaks with an enhanced magnetic transition temperature of $T_{C1} \sim 310$ K: (d) (0, 0, 9); (e) (1, 0, 0); and (f) (1, 0, 3).

The development of the AA-stacking order after the first cool process through T_S is also confirmed by our neutron diffraction study on another quenched F5GT single crystal [Figs. 3, 4, and 5(b)–5(d)]. The F5GT crystal was investigated following a similar temperature-dependent sequence: starting at RT, first cool to $T = 4$ K, and then warm up to 350 K (thermally cycled). Without first cool through T_S , the \mathbf{Q}_{AA} Bragg peaks, such as the (1, 0, 0), (1, 0, 3), and (1, 0, 6) reflections, are clearly absent [Figs. 3(b) and 5(b)]. In agreement with the ABC-stacking order, the \mathbf{Q}_{ABC} Bragg peaks, such as the (1, 0, 1) and (1, 0, 4) reflections, are observed as expected [Figs. 3(c), 3(d) and 5(b)]. Interestingly, after the sample was subjected to first cool to $T = 4$ K, it permanently entered the thermally cycled state with a different set of diffraction peaks. All of the \mathbf{Q}_{ABC} Bragg peaks observed before the structural transition at T_S , such as the (1, 0, 4) peak, completely vanish [Figs. 3(f) and 5(d)]. Meanwhile, the \mathbf{Q}_{AA} Bragg peaks initially absent, such as the (1, 0, 0) peak, are now clearly visible [Figs. 4(b), 4(c) and 5(d)]. This suggests the complete conversion from ABC-stacking order to AA-stacking order after the thermal-cycling process in this particular sample. The combined x-ray and neutron scattering data on the structural properties evidently indicate the F5GT sample experiences a structural alteration at T_S during the first cool process, in which the system either partially or completely converts from ABC-stacking order to AA-stacking order.

Having established this novel structural evolution in F5GT, the magnetic properties can also be re-evaluated from the neutron scattering data. Consistent with the early neutron powder diffraction study [10], the \mathbf{Q}_{ABC} Bragg peaks are both structural and magnetic in origin [Figs. 3(c), 3(d) and

5(b)], confirming the FM nature of the magnetic order. For instance, both the (1, 0, 1) and (1, 0, 4) reflections display temperature dependencies with a magnetic onset temperature of $T_{C0} \sim 274$ K [Figs. 3(e) and 3(f)], which is slightly lower than the value from the magnetization data of the other F5GT sample. Since the magnetic neutron scattering intensity is only sensitive to the spin moment component perpendicular to the scattering vector \mathbf{Q} [32], the absence of magnetic peaks at the (0, 0, $3N$) ($N = 1, 2, \dots$) positions, such as at (0, 0, 9) in Fig. 3(a), confirms the out-of-plane spin moment direction in F5GT with ABC-stacking order. When this particular sample is thermally cycled with the complete AA-stacking order, the magnetic peaks appear with a different pattern. Again, both the \mathbf{Q}_{AA} and (0, 0, $3N$) reflections are structural and magnetic, and they demonstrate the temperature dependence with an enhanced onset temperature of $T_{C1} \sim 310$ K [Figs. 4, 5(c), and 5(d)]. For instance, the (0, 0, 9) peak now develops strong intensity below T_{C1} [Figs. 4(a) and 4(d)], in stark contrast to its absence before the first cool treatment [Fig. 3(a)]. The observation of magnetic peaks at the (0, 0, $3N$) positions directly implies the existence of an in-plane spin moment component. Considering both the structural and the magnetic peaks residing at the same Bragg peak positions, and from the representational analysis [33], the magnetic moment direction is either purely in-plane or out-of-plane. Therefore, the presence of the magnetic peaks at the (0, 0, $3N$) positions in the AA-stacking order F5GT sample implies FM order with the spin moments oriented in-plane. Additionally, a simple FM model with the same spin moment size was used to calculate the magnetic structure factor squared for neutrons and to simulate the measured magnetic peak intensity, which results in

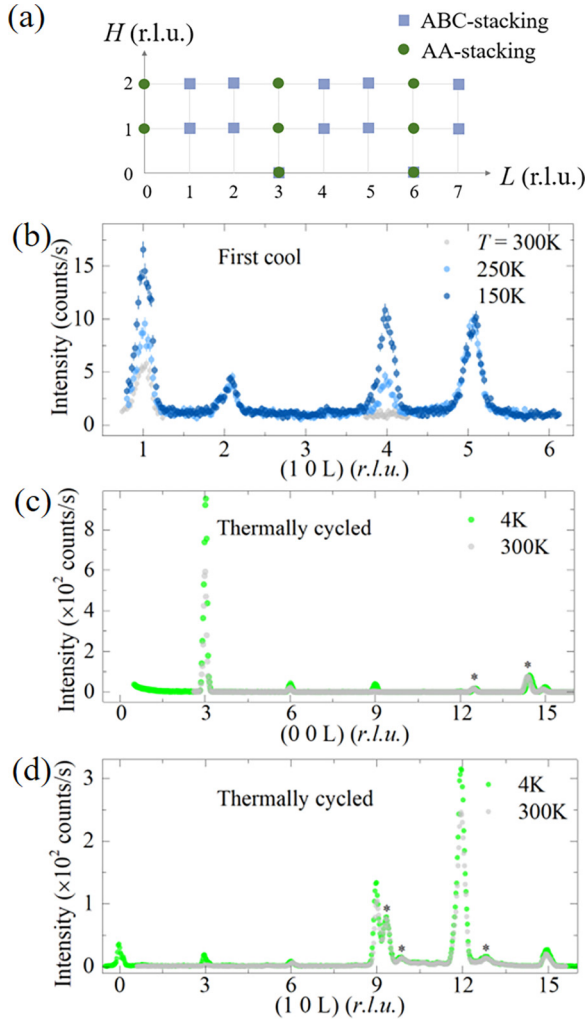


FIG. 5. (a) Schematic of the nuclear Bragg peak positions in the $(H, 0, L)$ plane of F5GT with two types of stacking orders, indexed with the same lattice parameters: ABC-stacking (blue squares) and AA-stacking (green circles). (b)–(d) Long L scans of the neutron diffraction peaks of F5GT at select temperatures, under different thermal statuses: first cool [panel (b)] and thermally cycled [panels (c) and (d)]. Peaks marked by asterisks are temperature-independent background from the aluminum holder.

an average spin moment size of $\sim 1.5(2) \mu_B/\text{Fe}$ (details about the calculation can be found in the Supplemental Material [34], Fig. S1). This value is slightly less than that obtained from the magnetization measurement ($\sim 2 \mu_B/\text{Fe}$) [26,28], but is close to estimated magnetic moments from other experimental probes and theoretical calculations [10,17,35,36].

To gain more insight about the nature of the magnetic transition in F5GT, power-law fitting of the order parameter squared [37–40], the peak intensity, is applied at select magnetic reflections in the temperature range from 200 K to near T_C (a constant is applied to account for the background and structural contributions, solid lines in Fig. 6) under the following form:

$$I \propto (T_C - T)^{2\beta}. \quad (1)$$

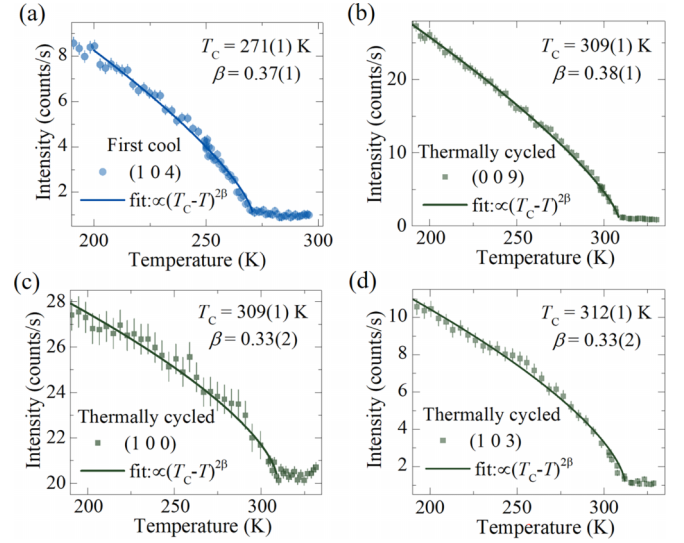


FIG. 6. Power-law fitting of the magnetic peak intensity at select Bragg peak positions in F5GT under different thermal statuses (solid lines): (a) first cool and (b)–(d) thermally cycled.

The power-law fit of the $(1, 0, 4)$ magnetic peak of ABC-stacked F5GT during the first cool process yields $T_C = 271(1)\text{K}$ and $\beta = 0.37(1)$ [Fig. 6(a)]. The fitted number $T_C = 271(1)\text{K}$, reflecting the bulk magnetic transition, is slightly lower than the number $T_{C1} \sim 285\text{K}$ obtained from magnetization data. This discrepancy can be understood because a small magnetic field applied to the system during the magnetization measurements, together with the local chemical inhomogeneity, produces some magnetic signals above $T_C = 271(1)\text{K}$, which therefore display a seemingly larger $T_{C0} \sim 285\text{K}$. Similarly, the power-law fits of the selected reflections of AA-stacked F5GT under thermally cycled status render $T_C \sim T_{C1} \sim 310\text{K}$ and $\beta = 0.33\text{--}0.38$ [Figs. 6(b)–6(d)]. The larger fitted value $T_C \sim 310\text{K}$ of AA-stacked F5GT is evident at all reflections signaling the bulk enhanced magnetic transition. Also, the fitted β numbers remain similar under different thermal treatments, as shown in Figs. 6(a) and 6(b), suggesting that, although the stacking sequences are altered, the magnetic phase transition behavior is not fundamentally modified. It is also worth noting that the averaged number $\beta = 0.35(3)$ is close to the value $\beta = 0.346(1)$ obtained via analyzing the temperature-dependent isothermal magnetization data [41]. We note that, because the spin anisotropy is weak in F5GT [11,13,17,36], we would expect a crossover from three-dimensional (3D) Heisenberg to either 3D Ising (ABC-stacking) or 3D XY (AA-stacking). In terms of the order parameter exponent, this implies a crossover from a value of $\beta = 0.366$ to either 0.326 or 0.347 [37,38]. Clearly our measured data are consistent with these values, but the uncertainties are too large to make a more precise statement.

III. DISCUSSION

Our combined x-ray and neutron scattering study clarifies that the thermal-history-dependent magnetization of the quenched F5GT sample results from the structural alteration upon the first cool procedure. Naturally, both the ABC-

stacking and the AA-stacking ordered domains may coexist within the thermally cycled sample. The presence of the AA-stacking order is not surprising. It is known that there exist stacking faults or structural disorder within the F5GT samples [9,10]. Comparing to the ABC-stacking order, the AA-stacking order keeps the in-plane building blocks while only differing slightly through the out-of-plane stacking configuration. Encouragingly, the density functional theory (DFT) calculation indicates that the ground-state energies for ABC, AA, and AA' [42] structural and magnetic phases lie within about ± 10 meV per formula unit [26], strongly supporting the idea that similar stacking configurations are experimentally accessible in F5GT. This is consistent with the fact that through electron doping in F5GT, the AA-stacking order is readily preferred [24,26–28]. Therefore, quenching the crystals during the last step of the synthesis may preferably freeze the population of the ABC-stacked domains, maintaining the “high quality” of the crystals. However, during the first cool procedure at $T_S \sim 110$ K (~ 9.5 meV), the spins at the Fe1 site start ordering [10]. Because of the strong magnetoelastic coupling and the interlayer exchange coupling, especially the spins at the outer Fe1 site, some domains convert from ABC-stacking to AA-stacking. However, this process may not go to completion because of other competing factors, such as (structural and chemical) disorder and/or Fe vacancies, that retain the ABC-stacked domains. This “permanent” change may be recycled and the population of the ABC- and AA-stacked domains may be redistributed, if the system is warmed up to 550 K and beyond [12].

From the neutron diffraction data (Figs. 3–5), it is evident that the two types of domains demonstrate contrasting magnetic behavior. Specifically, the ABC-stacked domains host out-of-plane moments with a lower FM transition temperature T_{C0} ; while the AA-stacked domains accommodate in-plane moments with an enhanced $T_{C1} \sim 310$ K [Figs. 1(a) and 1(b)]. While the spin moment directions of the ABC- and AA-stacked domains are different, the intralayer spin moments maintain strong FM exchange couplings. Also, the in-plane FM order observed in AA-stacked domains is not totally unexpected. Both the experimental data [11,17] and DFT calculations [13,36] have demonstrated a weak magnetic anisotropy in F5GT. Therefore, a small perturbation to the system, leading to altered interlayer exchange couplings, may be able to flip the spin moment direction and enhance the ordering temperature in F5GT. Hence, the in-plane FM order with an enhanced T_C is observed in AA-stacked domains, as similarly reported in both Co- and Ni-doped F5GT samples [24,28]. This can also explain the magnetic anisotropy control and the modulation of T_C in F5GT via the high-pressure diamond-anvil-cell technique [30]. With higher magnetic onset temperatures consistently recorded in Co- and Ni-doped FGT systems [24,26–28,43], the AA-stacking lattice structure seems to be favorable for increasing the magnetic ordering temperature.

Since the ground-state energies of the structural and magnetic phases in relevant polytypes of F5GT are close, as well as having a weak magnetic anisotropy, one might expect rich manipulations of the magnetic properties in F5GT. Even within one single crystal, because of local disorder and Fe vacancies, different types of domains might coexist, as revealed

from our x-ray scattering data in Fig. 2. From this perspective, the enhanced T_C and the anomalous critical exponent β extracted in some previous studies from the magnetization data resulting from coexisting domains may be understood [11,22]. Also, since the F5GT single crystals are produced with various sets of synthesis parameters from different groups, the magnetic properties will display some variations because of the distinct types of domains, including the out-of-plane FM [10,12,15,17–19,44], the in-plane FM [11,16], ferrimagnetism [16], or helical magnetism [14].

It is worth noting that the thermally cycled F5GT sample does not display a strong anomaly at T_S from our neutron diffraction data [Figs. 4(e) and 4(f)], as opposed to the temperature induced spin-flip transition implied from the magneto-transport measurements [30,45]. Conversely, the sister compound Fe_4GeTe_2 behaves strikingly similar to pre-cooled F5GT in magnetization, including a similar $T_C \sim 270$ K, as well as a spin reorientation at ~ 110 K [46,47]. Therefore, the inconsistent magnetic behavior may be ascribed to a possible Fe deficiency δ in F5GT [46,48]. Hence, it is crucial to characterize both the Fe deficiency level and the stacking order in F5GT [49], especially when measuring nanoflakes with a reduced sample thickness, in order to correctly interpret the magnetic properties.

Lastly, our work establishes effective protocols to monitor the stacking sequence and the magnetic state in F5GT, which can be extended to other layered vdW magnets. Particularly, the stacking configuration in F5GT is readily differentiated by inspecting the $\mathbf{Q} = (H, 0, L)$ ($H \neq 0$) type of nuclear Bragg peaks [Fig. 5(a)]. Meanwhile, measuring only the $(0, 0, L)$ type of reflections is not sufficient to fully characterize the various stacking arrangements, which might frequently occur in weakly vdW bonded materials.

IV. CONCLUSION

In summary, our combined x-ray and neutron scattering study of Fe_5GeTe_2 single crystals elucidates the thermal history dependence of the magnetization data of quenched F5GT. The irreversible, first-order structural transition at $T_S \sim 110$ K through the first cool process corresponds to a partial or complete alteration of the stacking order, from ABC-stacking order to AA-stacking order. The neutron scattering data establish the FM nature and indicate that the magnetic properties, such as the spin moment direction and the magnetic onset temperature, are determined by the stacking order: the ABC-stacking ordered domains host out-of-plane spin moments with a lower T_{C0} , while the AA-stacking order presents in-plane spin moments with an increased $T_{C1} \sim 310$ K. The neutron scattering data also are consistent with a 3D Heisenberg model and reveal an average spin moment size of $\sim 1.5(2) \mu_B/\text{Fe}$ in F5GT. Our work highlights the significant role of the stacking order of the lattice to the magnetism in F5GT, as well as the importance of the Fe deficiency in determining its magnetic ground state.

ACKNOWLEDGMENTS

Work at the University of California, Berkeley, and the Lawrence Berkeley National Laboratory was funded by the

U.S. Department of Energy, Office of Science, Office of Basic Energy Sciences, Materials Sciences and Engineering Division, under Contract No. DE-AC02-05-CH11231 within the Quantum Materials Program (KC2202). This work is based upon research conducted at the Center for High Energy X-ray

Sciences (CHEXS) which is supported by the National Science Foundation under Grant No. DMR-1829070. A portion of this research used resources at the High Flux Isotope Reactor, which is a DOE Office of Science User Facility operated by Oak Ridge National Laboratory.

- [1] J.-G. Park, Opportunities and challenges of 2D magnetic van der Waals materials: magnetic graphene? *J. Phys.: Condens. Matter* **28**, 301001 (2016).
- [2] K. S. Burch, D. Mandrus, and J.-G. Park, Magnetism in two-dimensional van der Waals materials, *Nature (London)* **563**, 47 (2018).
- [3] M. Gibertini, M. Koperski, A. F. Morpurgo, and K. S. Novoselov, Magnetic 2D materials and heterostructures, *Nat. Nanotechnol.* **14**, 408 (2019).
- [4] C. Gong and X. Zhang, Two-dimensional magnetic crystals and emergent heterostructure devices, *Science* **363**, eaav4450 (2019).
- [5] K. F. Mak, J. Shan, and D. C. Ralph, Van der Waals heterostructures for spintronics and opto-spintronics, *Nat. Rev. Phys.* **1**, 646 (2019).
- [6] J. F. Sierra, J. Fabian, R. K. Kawakami, S. Roche, and S. O. Valenzuela, Van der Waals heterostructures for spintronics and opto-spintronics, *Nat. Nanotechnol.* **16**, 856 (2021).
- [7] C. Gong, L. Li, Z. Li, H. Ji, A. Stern, Y. Xia, T. Cao, W. Bao, C. Wang, Y. Wang, Z. Q. Qiu, R. J. Cava, S. G. Louie, J. Xia, and X. Zhang, Discovery of intrinsic ferromagnetism in two-dimensional van der Waals crystals, *Nature (London)* **546**, 265 (2017).
- [8] B. Huang, G. Clark, E. Navarro-Moratalla, D. R. Klein, R. Cheng, K. L. Seyler, D. Zhong, E. Schmidgall, M. A. McGuire, D. H. Cobden, W. Yao, D. Xiao, P. Jarillo-Herrero, and X. Xu, Layer-dependent ferromagnetism in a van der Waals crystal down to the monolayer limit, *Nature (London)* **546**, 270 (2017).
- [9] J. Stahl, E. Shlaen, and D. Johrendt, The van der Waals ferromagnets $\text{Fe}_{5-\delta}\text{GeTe}_2$ and $\text{Fe}_{5-\delta-x}\text{Ni}_x\text{GeTe}_2$ crystal structure, stacking faults, and magnetic properties, *Z. Anorg. Allg. Chem.* **644**, 1923 (2018).
- [10] A. F. May, D. Ovchinnikov, Q. Zheng, R. Hermann, S. Calder, B. Huang, Z. Fei, Y. Liu, X. Xu, and M. A. McGuire, Ferromagnetism near Room Temperature in the Cleavable van der Waals Crystal Fe_5GeTe_2 , *ACS Nano* **13**, 4436 (2019).
- [11] H. Zhang, R. Chen, K. Zhai, X. Chen, L. Caretta, X. Huang, R. V. Chopdekar, J. Cao, J. Sun, J. Yao, R. Birgeneau, and R. Ramesh, Itinerant ferromagnetism in van der Waals $\text{Fe}_{5-x}\text{GeTe}_2$ crystals above room temperature, *Phys. Rev. B* **102**, 064417 (2020).
- [12] A. F. May, C. A. Bridges, and M. A. McGuire, Physical properties and thermal stability of $\text{Fe}_{5-x}\text{GeTe}_2$ single crystals, *Phys. Rev. Mater.* **3**, 104401 (2019).
- [13] X. Yang, X. Zhou, W. Feng, and Y. Yao, Strong magneto-optical effect and anomalous transport in the two-dimensional van der Waals magnets Fe_nGeTe_2 ($n = 3, 4, 5$), *Phys. Rev. B* **104**, 104427 (2021).
- [14] T. T. Ly, J. Park, K. Kim, H.-B. Ahn, N. J. Lee, K. Kim, T.-E. Park, G. Duvjir, N. H. Lam, K. Jang, C.-Y. You, Y. Jo, S. K. Kim, C. Lee, S. Kim, and J. Kim, Direct observation of Fe-Ge ordering in $\text{Fe}_{5-x}\text{GeTe}_2$ crystals and resultant helimagnetism, *Adv. Funct. Mater.* **31**, 2009758 (2021).
- [15] Y. Gao, Q. Yin, Q. Wang, Z. Li, J. Cai, T. Zhao, H. Lei, S. Wang, Y. Zhang, and B. Shen, Spontaneous (anti)meron chains in the domain walls of van der Waals ferromagnetic $\text{Fe}_{5-x}\text{GeTe}_2$, *Adv. Mater.* **32**, 2005228 (2020).
- [16] L. Alahmed, B. Nepal, J. Macy, W. Zheng, B. Casas, A. Sapkota, N. Jones, A. R. Mazza, M. Brahlek, W. Jin, M. Mahjouri-Samani, S. S.-L. Zhang, C. Mewes, L. Balicas, T. Mewes, and P. Li, Magnetism and spin dynamics in room-temperature van der Waals magnet Fe_5GeTe_2 , *2D Mater.* **8**, 045030 (2021).
- [17] M. Ribeiro, G. Gentile, A. Marty, D. Dosenovic, H. Okuno, C. Vergnaud, J.-F. Jacquot, D. Jalabert, D. Longo, P. Ohresser, A. Hallal, M. Chshiev, O. Boulle, F. Bonell, and M. Jamet, Large-scale epitaxy of two-dimensional van der Waals room-temperature ferromagnet Fe_5GeTe_2 , *npj 2D Mater. Appl.* **6**, 10 (2022).
- [18] G. K. R. Nair, Z. Zhang, F. Hou, A. Abdelaziem, X. Xu, S. W. Q. Yang, N. Zhang, W. Li, C. Zhu, Y. Wu, H. Weiling, L. Kang, T. Salim, J. Zhou, L. Ke, J. Lin, X. Li, W. Gao, and Z. Liu, Phase-pure two-dimensional Fe_xGeTe_2 magnets with near-room-temperature T_C , *Nano Res.* **15**, 457 (2022).
- [19] H. Chen, S. Asif, M. Whalen, J. Támara-Isaza, B. Luetke, Y. Wang, X. Wang, M. Ayako, S. Lamsal, A. F. May, M. A. McGuire, C. Chakraborty, J. Q. Xiao, and M. J. H. Ku, Revealing room temperature ferromagnetism in exfoliated Fe_5GeTe_2 flakes with quantum magnetic imaging, *2D Mater.* **9**, 025017 (2022).
- [20] K. Yamagami, Y. Fujisawa, B. Driesen, C. H. Hsu, K. Kawaguchi, H. Tanaka, T. Kondo, Y. Zhang, H. Wadati, K. Araki, T. Takeda, Y. Takeda, T. Muro, F. C. Chuang, Y. Niimi, K. Kuroda, M. Kobayashi, and Y. Okada, Itinerant ferromagnetism mediated by giant spin polarization of the metallic ligand band in the van der Waals magnet Fe_5GeTe_2 , *Phys. Rev. B* **103**, L060403 (2021).
- [21] X. Wu, L. Lei, Q. Yin, N.-N. Zhao, M. Li, Z. Wang, Q. Liu, W. Song, H. Ma, P. Ding, Z. Cheng, K. Liu, H. Lei, and S. Wang, Direct observation of competition between charge order and itinerant ferromagnetism in the van der Waals crystal $\text{Fe}_{5-x}\text{GeTe}_2$, *Phys. Rev. B* **104**, 165101 (2021).
- [22] K. Yamagami, Y. Fujisawa, M. Pardo-Almanza, B. R. M. Smith, K. Sumida, Y. Takeda, and Y. Okada, Enhanced $d-p$ hybridization intertwined with anomalous ground state formation in the van der Waals itinerant magnet Fe_5GeTe_2 , *Phys. Rev. B* **106**, 045137 (2022).
- [23] K. Huang, Z. Li, D. Guo, H. Yang, Y. Li, A. Liang, F. Wu, L. Xu, L. Yang, W. Ji, Y. Guo, Y. Chen, and Z. Liu, Measurement of electronic structure in van der Waals ferromagnet $\text{Fe}_{5-x}\text{GeTe}_2$, *Chin. Phys. B* **31**, 057404 (2022).

- [24] A. F. May, M.-H. Du, V. R. Cooper, and M. A. McGuire, Tuning magnetic order in the van der Waals metal Fe_5GeTe_2 by cobalt substitution, *Phys. Rev. Mater.* **4**, 074008 (2020).
- [25] C. Tian, F. Pan, S. Xu, K. Ai, T. Xia, and P. Cheng, Tunable magnetic properties in van der Waals crystals $(\text{Fe}_{1-x}\text{Co}_x)_5\text{GeTe}_2$, *Appl. Phys. Lett.* **116**, 202402 (2020).
- [26] H. Zhang, Y.-T. Shao, R. Chen, X. Chen, S. Susarla, D. Raftrey, J. T. Reichanadter, L. Caretta, X. Huang, N. S. Settinieri, Z. Chen, J. Zhou, E. Bourret-Courchesne, P. Ercius, J. Yao, P. Fischer, J. B. Neaton, D. A. Muller, R. J. Birgeneau, and R. Ramesh, A room temperature polar magnetic metal, *Phys. Rev. Mater.* **6**, 044403 (2022).
- [27] H. Zhang, D. Raftrey, Y.-T. Chan, Y.-T. Shao, R. Chen, X. Chen, X. Huang, J. T. Reichanadter, K. Dong, S. Susarla, L. Caretta, Z. Chen, J. Yao, P. Fischer, J. B. Neaton, W. Wu, D. A. Muller, R. J. Birgeneau, and R. Ramesh, Room-temperature skyrmion lattice in a layered magnet $(\text{Fe}_{0.5}\text{Co}_{0.5})_5\text{GeTe}_2$, *Sci. Adv.* **8**, eabm7103 (2022).
- [28] X. Chen, Y.-T. Shao, R. Chen, S. Susarla, T. Hogan, Y. He, H. Zhang, S. Wang, J. Yao, P. Ercius, D. A. Muller, R. Ramesh, and R. J. Birgeneau, Pervasive beyond Room-Temperature Ferromagnetism in a Doped van der Waals Magnet, *Phys. Rev. Lett.* **128**, 217203 (2022).
- [29] C. Tan, W.-Q. Xie, G. Zheng, N. Aloufi, S. Albarakati, M. Algarni, J. Li, J. Partridge, D. Culcer, X. Wang, J. B. Yi, M. Tian, Y. Xiong, Y.-J. Zhao, and L. Wang, Gate-controlled magnetic phase transition in a van der Waals magnet Fe_5GeTe_2 , *Nano Lett.* **21**, 5599 (2021).
- [30] Z. Li, M. Tang, J. Huang, F. Qin, L. Ao, Z. Shen, C. Zhang, P. Chen, X. Bi, C. Qiu, Z. Yu, K. Zhai, T. Ideue, L. Wang, Z. Liu, Y. Tian, Y. Iwasa, and H. Yuan, Magnetic anisotropy control with Curie temperature above 400 K in a van der Waals ferromagnet for spintronic device, *Adv. Mater.* **34**, 2201209 (2022).
- [31] Y. Gao, S. Yan, Q. Yin, H. Huang, Z. Li, Z. Zhu, J. Cai, B. Shen, H. Lei, Y. Zhang, and S. Wang, Manipulation of topological spin configuration via tailoring thickness in van der Waals ferromagnetic $\text{Fe}_{5-x}\text{GeTe}_2$, *Phys. Rev. B* **105**, 014426 (2022).
- [32] G. L. Squires, *Introduction to the Theory of Thermal Neutron Scattering* (Cambridge University, Cambridge, England, 1978).
- [33] A. Wills, A new protocol for the determination of magnetic structures using simulated annealing and representational analysis (SARAh), *Phys. B: Condens. Matter* **276-278**, 680 (2000).
- [34] See Supplemental Material at <http://link.aps.org/supplemental/10.1103/PhysRevMaterials.7.044411> for more details about the determination of the spin moment size in Fe_5GeTe_2 .
- [35] M. Joe, U. Yang, and C. Lee, First-principles study of ferromagnetic metal Fe_5GeTe_2 , *Nano Mater. Sci.* **1**, 299 (2019).
- [36] S. Ershadrad, S. Ghosh, D. Wang, Y. Kvashnin, and B. Sanyal, Unusual magnetic features in two-dimensional Fe_5GeTe_2 induced by structural reconstructions, *J. Phys. Chem. Lett.* **13**, 4877 (2022).
- [37] R. Guida and J. Zinn-Justin, Critical exponents of the N -vector model, *J. Phys. A: Math. Gen.* **31**, 8103 (1998).
- [38] A. Pelissetto and E. Vicari, Critical phenomena and renormalization-group theory, *Phys. Rep.* **368**, 549 (2002).
- [39] R. J. Birgeneau, J. Als-Nielsen, and G. Shirane, Critical behavior of pure and site-random two-dimensional antiferromagnets, *Phys. Rev. B* **16**, 280 (1977).
- [40] X. Chen, Y. He, S. Wu, Y. Song, D. Yuan, E. Bourret-Courchesne, J. P. C. Ruff, Z. Islam, A. Frano, and R. J. Birgeneau, Structural and magnetic transitions in the planar antiferromagnet $\text{Ba}_4\text{Ir}_3\text{O}_{10}$, *Phys. Rev. B* **103**, 224420 (2021).
- [41] Z. Li, W. Xia, H. Su, Z. Yu, Y. Fu, L. Chen, X. Wang, N. Yu, Z. Zou, and Y. Guo, Magnetic critical behavior of the van der Waals Fe_5GeTe_2 crystal with near room temperature ferromagnetism, *Sci. Rep.* **10**, 15345 (2020).
- [42] The AA' stacking order is achieved in 50% Co-doped F5GT, which might be useful for spintronic applications.
- [43] X. Chen, E. Schierle, Y. He, M. Vranas, J. W. Freeland, J. L. McChesney, R. Ramesh, R. J. Birgeneau, and A. Frano, Antiferromagnetic order in Co-doped Fe_5GeTe_2 probed by resonant magnetic x-ray scattering, *Phys. Rev. Mater.* **6**, 094404 (2022).
- [44] M. Schmitt, T. Denneulin, A. Kovács, T. G. Saunderson, P. Rützmann, A. Shahee, T. Scholz, A. Tavabi, M. Gradhand, P. Mavropoulos, B. V. Lotsch, R. E. Dunin-Borkowski, Y. Mokrousov, S. Blügel, and M. Kläui, Skyrmionic spin structures in layered Fe_5GeTe_2 up to room temperature, *Commun. Phys.* **5**, 254 (2022).
- [45] Z. Li, K. Huang, D. Guo, G. Ma, X. Liu, Y. Wu, J. Yuan, Z. Tao, B. Wang, X. Wang *et al.*, Weak antilocalization effect up to ~ 120 K in the van der Waals crystal $\text{Fe}_{5-x}\text{GeTe}_2$ with near room temperature ferromagnetism, [arXiv:2109.02085](https://arxiv.org/abs/2109.02085).
- [46] J. Seo, D. Y. Kim, E. S. An, K. Kim, G.-Y. Kim, S.-Y. Hwang, D. W. Kim, B. G. Jang, H. Kim, G. Eom, S. Y. Seo, R. Stania, M. Muntwiler, J. Lee, K. Watanabe, T. Taniguchi, Y. J. Jo, J. Lee, B. I. Min, M. H. Jo *et al.*, Nearly room temperature ferromagnetism in a magnetic metal-rich van der Waals metal, *Sci. Adv.* **6**, eaay8912 (2020).
- [47] S. Mondal, N. Khan, S. M. Mishra, B. Satpati, and P. Mandal, Critical behavior in the van der Waals itinerant ferromagnet Fe_4GeTe_2 , *Phys. Rev. B* **104**, 094405 (2021).
- [48] Q. Liu, J. Xing, Z. Jiang, Y. Guo, X. Jiang, Y. Qi, and J. Zhao, Layer-dependent magnetic phase diagram in Fe_nGeTe_2 ($3 \leq n \leq 7$) ultrathin films, *Commun. Phys.* **5**, 140 (2022).
- [49] N. Sivasdas, S. Okamoto, X. Xu, C. J. Fennie, and D. Xiao, Stacking-dependent magnetism in bilayer CrI_3 , *Nano Lett.* **18**, 7658 (2018).